Journal of Materials Chemistry A

Accepted Manuscript

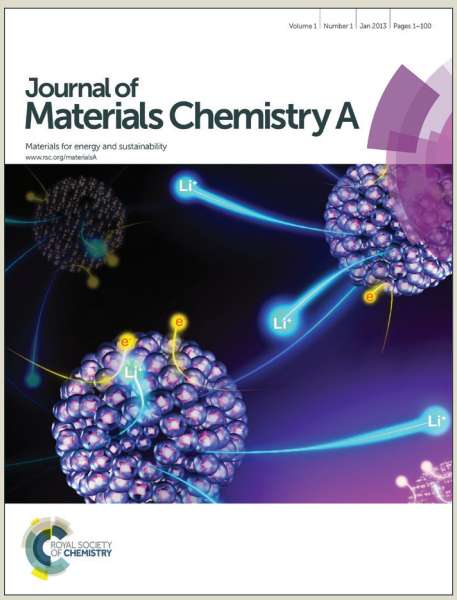

ROYAL SOCIETY OF CHEMISTRY

www.rsc.org/materialsA

Journal Name

ARTICLE

Vertically aligned, double-sided, and self-supported 3D WO_3 nanocolumn bundles for low-temperature gas sensing

Received 00th January 20xx,
Accepted 00th January 20xx

DOI: 10.1039/x0xx00000x

www.rsc.org/

J. J. Qi,[a] S. Gao,[a] K. Chen,[a] J. Yang,[a] H. W. Zhao,[a] L. Guo*[a] and S. H. Yang*[b]

A three-dimensional (3D) hierarchical structure consisting of vertically bundled, double-sided, and self-supported WO_3 nanocolumn bundles has been successfully synthesized via acid-assisted (HCl) hydrothermal process without any templates, catalysts, or substrates. A possible formation mechanism is proposed, which involves dissolution–recrystallization and Ostwald ripening processes in concert with the structure-directing role of HCl, leading to the morphology grown along [200] with largely exposed (002) facets. The hierarchical monoclinic structure of WO_3–based sensor contains abundant active sites and loose structures beneficial conditions for gas adsorption and diffusion, which prove to be an excellent NO_2-sensing material with high sensitivity, good selectivity, rapid response (*ca.* 23 s) / recovery (*ca.* 11 s), and remarkable repeatability at a low operating temperature (~110 °C). A possible gas-sensing mechanism will be discussed based on largely exposed (002) facets, which the O-terminated (001) surface containing unsaturated coordinated O atoms is more active to adsorb NO_2 molecules easily and efficiently. The superior gas sensor properties offer a potential platform for monitoring harmful and toxic gases, especially those flammable and explosive volatile organic compounds (VOCs).

1. Introduction

In modern times, the toxic and hazardous gas emissions have dramatically increased with the rapid economic growth and industrialization. In particular, nitrogen dioxide (NO_2) as one of the primary source of photochemical smog and acid rain has aroused public attention. To effectively detect the hazardous gas, gas sensors are recognized as the most effective devices owing to their high sensitivity, fast response, and excellent selectivity,[1-4] which strongly demands on the gas-sensing materials.[5, 6] Among various gas sensor materials studied so far, tungsten oxide (WO_3) is an important n-type semiconductor with wide band-gap of ~ 2.7 eV, which has attracted extensive interest due to its numerous potential applications in electrochromic materials,[7-9] photocatalysts,[10-12] lithium batteries,[13] electrodes for solar cells,[14-17] and especially for remarkable gas sensing properties to detect NO_2 gas or volatile organic compounds (VOCs).[18-20]

It is well-known that the sensing mechanism belongs to the surface controlled type containing the parameters (*e.g.,* size, dimensionality, morphology, crystal phase, crystallinity, and surface states)[21] which have profound influence on the WO_3-based gas sensing properties.[22] Hence, many researchers have mainly focused on low-dimensional structures with enhancing the material performance (*e.g.*, 0D (zero-dimensional), 1D, 2D),[23-27] but relatively few studies have reported on novel three-dimensional (3D) assembled[17]/hierarchical architectures (flowers,[16] trees[28]) for gas sensing, which synthesized by using a series of physical and chemical methods, including microwave hydrothermal processes,[29] chemical vapor deposition (CVD),[30] sol-gel approaches,[31] and hydrothermal reactions.[6] Therefore, hierarchical micro/nano structures assembled by using low-dimension particles, rods, wires, or sheets etc. as building blocks[32] with facile prepared method attract more and more research interests owing to their less gas diffusion length, higher mobility, and relatively larger specific surface area than that the agglomerated nanocrystals.[33] However, up to now, it is still a great challenge to realize the fabrication of hierarchical 3D WO_3 by assembling the 1D/2D WO_3 nanostructures using a facile route. Besides, the relationship between 3D WO_3 with special morphologies and enhancing gas-sensing properties has not been understood very well yet.

Herein, we report a facile one-pot hydrothermal approach for synthesis of three-dimensional (3D) hierarchical structure of vertically aligned, double-sided, and self-supported WO_3 nanocolumn bundles at 180 °C for 15 h. Moreover, the evolutionary process of the morphology is rationally proposed on the basis of dissolution-recrystallization and Ostwald ripening processes with HCl directing the morphology grown along [200] with largely exposed (002) facets. Balancing the hydrolysis and recrystallization rates of the WCl_6 precursors through precisely adjusting the experimental parameters is the key to success. Finally, the hierarchical monoclinic structure of WO_3-based sensor contains abundant active sites and loose structures beneficial conditions for gas adsorption and diffusion, which prove to be an excellent NO_2-sensing material with high sensitivity, good selectivity, rapid response (*ca.* 23 s) / recovery (*ca.* 11 s), and remarkable repeatability at a low operating temperature (~ 110 °C). A possible gas-sensing

[a] *School of Chemistry and Environment, Beihang University, Beijing 100191, China*
[b] *Department of Chemistry, The Hong Kong University of Science and Technology, Clear Water Bay, Kowloon, Hong Kong, China*
† *Corresponding author. E-mail: guolin@buaa.edu.cn; chsyang@ust.hk.*
Electronic Supplementary Information (ESI) available: [Supporting figures and some results and discussion]. See DOI: 10.1039/x0xx00000x

mechanism will be discussed based on largely exposed (002) facets, which the O-terminated (001) surface containing unsaturated coordinated O atoms is more active to adsorb NO_2 molecules easily and efficiently. These excellent gas-sensing properties will make our sample apply to the detection of toxic pollutant, combustible gases and organic vapors in gas sensors.

2. Experimental section

2.1 Synthetic procedures

The 3D hierarchical structures are synthesized via acid-assisted (HCl) hydrothermal process without any templates, catalysts, or substrates. In a typical reaction, a solution was prepared by adding 1.5 mL of concentrated hydrochloric acid (36.5 wt%-38 wt%) into the ethanol/distilled water (56 mL, 50/6, V/V) with stirring for 10 min at room temperature. Then, 10 mL of ethanol solution of 1.0 g tungsten chloride (WCl_6, Aladdin, 99.9%) as tungsten source was dropwise added to the above solution under vigorous stirring, and the color of the solution turned deep blue immediately with the WCl_6 addition. Besides, for another 1 h maintained room conditions for a precipitation process, the resulting solution was transferred to a 100 mL Teflon-lined stainless autoclave and heated at 180 °C for 15 h. After natural cooling to room temperature, the products were then collected by centrifuging and washed with distilled water and ethanol several times until the remaining ions in the products were removed, and dried at 60 °C. Finally, the sample was annealed at 300 °C in a muffle furnace for 2 h, and then detected their gas sensing properties to NO_2. Controlled experiments were performed for comparison, so as to find out the reactions of changing each experimental parameter while other conditions remained the same.

2.2 Characterization

Microscopic features of samples were characterized by Environmental scanning electron microscopy (ESEM, FEI Quanta 250 FEG) with the acceleration voltage of 10 kV. Transmission electron microscopy (TEM) and high-resolution TEM (HRTEM) studies were performed using JEOL JEM-2100F electron microscopes. The powder X-Ray diffraction (XRD) patterns of the samples were recorded by the Rigaku Dmax 2200 X-ray diffractometer with Cu Kα radiation (λ=1.5416 Å). The patterns were recorded at a scanning rate of 2 °min^{-1} within the range of 20-50° (2θ). Raman spectroscopy was studied on a laser Raman spectrometer (LabRAM HR800) using a visible laser (λ=532 nm) at room temperature. Nitrogen adsorption–desorption isotherm were measured by a NOVA2200e analyzer (Quntachrome, USA). Samples were degassed at 200 °C for 5 h before measurements.

2.3 Gas-sensing measurements

Mixing the samples with ethanol to form paste, and then drop-coated onto the surface of a ceramic tube with four Pt electrodes for several times, until a complete coating formed. The WO_3-coated ceramic tube was then welded on to a special six polar pedestal with solder paste. Then a small Ni-Cr heating coil was inserted through the ceramic tube with its two ends welded to the other two poles. The sensor elements were aged at 80 °C for several days to improve stability. The sensing performance was measured by a WS-30A test system (Weisheng Instruments Co., Zhengzhou, China). The as-prepared and annealed samples were carried out by testing the different concentrations of target gas to study the sensing properties. Operating temperature of the gas sensor was controlled by adjusting the heating voltage through an electric heating system. By monitoring the output voltage (V_{out}), we can measure both the resistance of the sensor in air (R_{air}) and in test target gas (R_{gas}). The sensor sensitivity (S) of NO_2 was defined as the ratio of R_{gas}/R_{air} (S = R_g/R_a), while the sensitivity of acetone was defined as the ratio of R_a/R_g. As the time for the sensor output to reach 90 % of its maximum response with switching on or off the gas in a step function was defined as response and recovery time, respectively.

3. Results and discussion

3.1 Morphology and structure

Typical ESEM images of the as-prepared WO_3 samples at different magnifications and perspectives are shown in Fig. 1. From the overall view image (Fig. 1a), it can be found that the obtained samples are almost entirely of diamond-shaped 3D WO_3, and the structures possess uniform morphology and size. The magnified front image (Fig. 1b) reveals a close-up one single WO_3 crystal with the length of ~ 7 μm and width of ~ 5 μm with some nanocolumn bundles in center (yellow dashed circle, see high-magnifications front view in Fig. 1c). The high-magnification SEM profile view as shown in Fig. 1d clearly presents the edge of the 3D WO_3 hierarchal structure is constructed by some nanocolumn bundles or sheet-like shapes growing in two opposite directions from the center, so the morphology of vertically aligned, double-sided and self-supported 3D WO_3 nanocolumn bundles has been successfully synthesized.

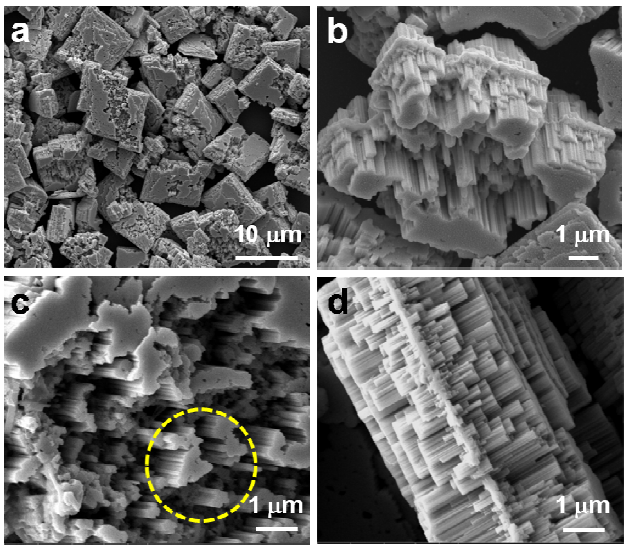

Fig. 1 ESEM images of the as-prepared WO_3 samples at different magnifications: (a) a panorama, (b) a close-up of one typical single crystal, (c) front view, and (d) profile view.

Besides, after annealing the sample at 300 °C for 2 h, the morphology of the sample shows no noticeable difference with that of as-prepared. The panorama (Fig. S1a†), front (Fig. S1b†), and profile (Fig. S1c†) SEM image shows that the structure and morphology still maintains. For better understanding the morphology of 3D WO_3 nanocolumn bundles, different analysis are presented and discussed in the following.

The crystal structure of the as-prepared powder is analyzed by XRD. As can be observed from Fig. 2a, all diffraction peaks can be readily indexed to the monoclinic WO_3 structures with the lattice parameters of a = 0.7297 nm, b = 0.7539 nm, c =0.7688 nm and the space group P21/*n* (JCPDS card no. 43-1035).[17] The dominant peaks at 2θ=23.11, 23.51 and 24.31 correspond to (002), (020) and (200) diffraction peak of typical monoclinic WO_3, respectively. Furthermore, the same results are also found in the sample annealed at 300 °C from the typical XRD patterns, as shown in Fig. S2a†, which means that there is no phase transition after the annealing process but merely with the diffraction peaks become stronger and sharper. The result also indicates that the annealed WO_3 sample has higher purity in crystalline phase than that of as-prepared, which may lead to enhance their properties. The diffraction intensity ratio of (002) facets to (200) facets (*i*.e., ($I_{(002)}/I_{(200)}$) of annealed WO_3 sample and as-prepared products is 4.17 and 2.47, respectively, which relatively enhanced compared to the verified standard pattern ($I_{(002)}/I_{(200)}$=1.01).[33] As calculated by the relative texture coefficient of a certain crystal facet (TC_{hkl}),[34] which is defined to evaluate the degree of the crystal facet exposure, the result is TC_{002} of annealed WO_3 sample and as-prepared products is 0.81 and 0.71, respectively. Thus, both results discussed above indicate that our structure exposes a larger proportion of (002) facets. The phase structure is also confirmed by Raman spectra, as shown in Fig. 2b.The bands at 804 and 714 cm^{-1} can be ascribed to the W-O stretching frequencies, and the bands located at 325 and 269 cm^{-1} are assigned to W-O-W bending mode of the bridging oxygen of the monoclinic phase which are consistent with the Raman shift reported in the literature.[16, 30] The results indicate that our prepared WO_3 sample possess monoclinic γ-phase structure.

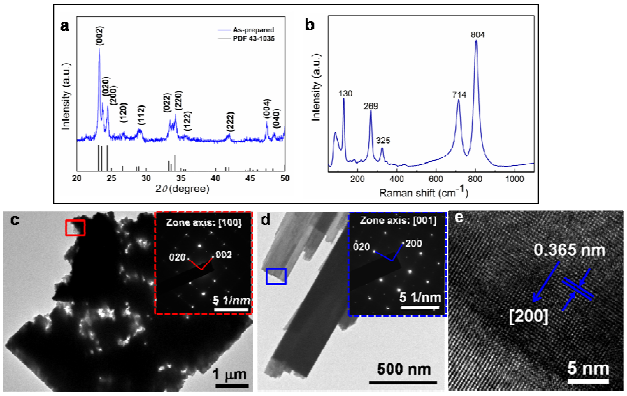

Fig. 2 (a) XRD pattern; (b) room temperature Raman spectrum; (c) low-magnification front projection TEM image, and the inset is the corresponding SAED pattern of the red rectangle; (d) low-magnification profile TEM image of the WO_3 nanocolumn, and the inserted SAED pattern of the blue rectangle; (e) the corresponding HRTEM image in the blue rectangle in d.

A detailed characterization of the microstructure information of 3D WO_3 nanocolumn bundles is conducted by TEM and HRTEM analysis. Fig. 2c shows a low-magnification front projection TEM image of 3D WO_3, exhibiting a single vertically aligned and self-supported 3D WO_3 microstructure, which consist with the SEM results (Fig. 1b). The corresponding selected area electron diffraction (SAED) pattern of the red rectangle inserted in Fig. 2c reveals that the single crystalline nature based on the ordered bright diffraction spots and the pattern can be recorded along the [100] zone axis of our 3D WO_3. In order to provide additional evidence of the crystal preferential growth orientation, the profile HRTEM image (Fig. 2e) and the corresponding inserted SAED pattern which selected from the low-magnification TEM image as the blue rectangle in Fig.2d indicates that the lattice fringes with the *d*-spacing of 0.365 nm agree well with the interplanar distances of (200) lattice planes of monoclinic WO_3 (JCPDS no.43-1035), confirming the morphology grown along [200].

3.2 Possible Growth mechanism of the self-supported 3D WO_3 nanocolumn bundles.

To reveal the possible growth mechanism of the vertically aligned, double-sided, and self-supported 3D WO_3 nanocolumn bundles, we carried out the important time-dependent experiments with the purpose of monitoring the morphology evolution process, during which samples are collected at different time intervals (0 h, 1 h, 10 h, and 15 h). As illustrated in Fig. 3a, there are four evolutionary stages of growth: (i) in the initial stage, (0 h, collecting the samples without hydrothermal treatment, Fig. 3b), no the mentioned special morphology is found, except lots of amorphous primary nanoparticles. Such a process involves a fast nucleation of amorphous primary small particles followed by a slow process of aggregation and crystallization of primary particles. (ii) With the reaction time proceeding (1 h, Fig. 3c), the morphology of the sample exhibits a certain thick and rough surface plate-like with a diameter of ~ 3 μm. Owing to adding the HCl in the reaction to form strong acid synthetic system (pH=0.5), on the one hand, the hydrolysis rate of WCl_6 precursors slow down, according to the reaction formula (the process of the reactions can be described as follows: $WCl_6 + nC_2H_5OH \rightarrow W(C_2H_5O)_nCl_{6-n} + nHCl$ and $WCl_6 + 4H_2O \rightarrow WO_3 \cdot H_2O + 6HCl$); on the other hand, the rough surface indicates the acid start directing the plates transform to arrays from this stage. That is, HCl may play a role of selective adsorption or capping agent and control the growth rate of various faces of WO_3 through adsorption on the rough surface in certain directions, leading to form the arrays structures, which are probably formed with a similar mechanism with WO_3 nanoplates.[35] At this second stage includes dissolution–recrystallization process and further growth processes, the tiny nuclei composed of the plate-like microstructures with rough surface results in an oriented nanocolumn bundles. (iii) When the reaction time is prolonged to 10 h with HCl directing the structure, then the intermediates appear, which are close to the final products assembled by nanocolumn bundles (the SEM images are shown in Fig. 3d), but have smaller size and thickness. During the orientated growth process, the dominant growth in two directions seems to be controlled by the intrinsic crystal orientations.

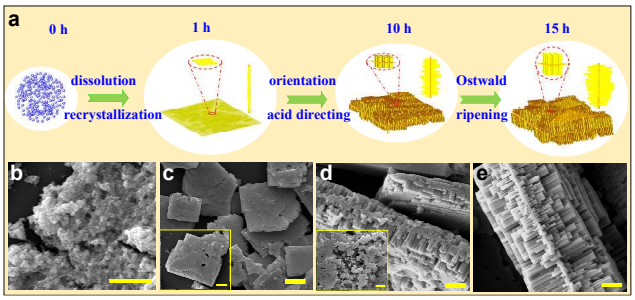

Fig. 3 Schematic illustration of the possible formation mechanism for the vertically aligned, double-sided, and self-supported WO_3 nanocolumn bundles. All the scale bars are 1 μm.

(iv) Finally, the typical morphology of vertically aligned, double-sided and self-supported 3D WO_3 nanocolumn bundles with a certain thickness has been obtained at reaction time of 15 h (Fig. 3e) through the Ostwald ripening process with existing HCl. In a word, HCl may play a crucial role in directing structure and slowing down the hydrolysis rate to form the special morphology. In this case, we suggest that our special 3D WO_3 are successfully synthesized due to the crystal preferential growth orientation along the [200] directions in the presence of HCl. To further demonstrate our assumption and comprehend the function of acid (HCl) on the synthetic process, the elaborate experiments on increasing amount of acid are considered in the solution, as illustrated and expounded in Fig. S3†.

3.3 Gas-sensing properties

We investigate the gas sensing properties of 3D hierarchical structures WO_3 for detecting NO_2, as shown in Fig. 4. Fig. 4a shows response of the sensors based on 3D WO_3 at different operating temperatures to 10 ppm NO_2 and 10 ppm acetone as a function of operating temperatures. For the samples annealed at 300 °C (red line), the sensitivity increases continuously with the operating temperature in the range of 25 to 110 °C, and then decreases, matching with the as-prepared samples (blue line). Thus, the optimum operating temperature is 110 °C and relatively lower comparing with that have been reported.[6, 36, 37] And the maximum sensitivity reaches 20.5 is about twice higher than that of the as-prepared samples at same testing condition. The response of the WO_3 at different annealed temperatures at optimum operating temperatures of 110 °C to 10 ppm NO_2 is also shown in the Fig. S4†. Fig. 4a the green line (the inset in Fig. 4a) shows the responses of the annealed sample to 10 ppm acetone at different operating temperatures. It can be found that the sensitivity reduces and the optimum operating temperature increases from 110 to 140 °C compared to the detecting NO_2 sensor. Therefore, it is obvious that operating temperature has a remarkable influence on the sensitivity of gas sensor, which has been proved by other reports. [6, 38] In general, when the operating temperature varies, the kinetics of adsorption and chemical reactions occurring at the sensor surface is altered, leading to the alteration of sensor sensitivity. However, if the temperature further increased, the sensor response decreases owing to the amount of adsorbed gas on the sensor surface will decrease, while the desorption process becomes dominant with increasing the operating temperature.

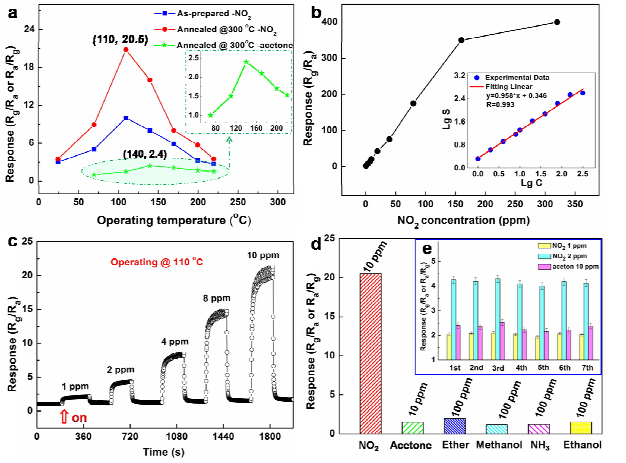

Fig. 4 (a) Response of the WO_3 at different operating temperatures: (blue line) As-prepared to 10 ppm NO_2; (red line) Annealed samples at 300 °C to 10 ppm NO_2; (green line) Annealed samples at 300 °C to 10 ppm acetone. (b) Response of WO_3 sensors based on the samples annealed at 300 °C to different NO_2 concentrations at 110 °C. Inset: the corresponding dilogarithm fit curve. (c) Transient responses of WO_3 annealed at 300 °C to 1-10 ppm NO_2 concentrations at 110 °C. (d) Response of the samples annealed at 300 °C to various gases at 110 °C. (e) The repeatability of WO_3 sensor to 1 ppm NO_2 at 110 °C, 2 ppm NO_2 at 110 °C, and 10 ppm acetone at 140 °C for seven cycles.

Fig. 4b shows the sensitivity of WO_3 sensors based on the samples annealed at 300 °C to different NO_2 concentration. It can be found that the response increases with the NO_2 concentration from 1 to 320 ppm, especially when the NO_2 concentration from 1-10 ppm, the response increases nearly linearly from 2.06 to 20.5 (the transient responses-time data as shown in Fig. 4c). When exposed to 20, 40, 80, 160, and 320 ppm NO_2, our WO_3-based sensor exhibits the response of 43, 75.5, 175, 350, and 400, respectively, proving a high concentration of gas sensing properties to hazardous NO_2 gas in the environment. Due to the response for detecting 100 ppb or 500 ppb NO_2 is too slight as shown in Fig. S5a†, indicating that our WO_3 sensor are advantageous in detecting ppm-level NO_2. According to previous reports,[39] such sensing response of the semiconductor oxide gas sensor as an irreversible process, Langmuir-Hinshelwood (L-H) reaction mechanism[40] has been used to illustrate the surface reaction on the sensing material. And an empirically representation of gas sensor response is as follows: $S=1 + A_g(P_g)^{\beta}$, where S is the sensor sensitivity, A_g denotes a prefactor, P_g is the partial pressure of the target gas, and β is the exponent on P_g. In general, P_g is directly proportional to the concentration of the detecting gas. Therefore, the logarithm of sensitivity (S) can be linear with the logarithm of the gas concentration (C). The fit curve of the Lg (S) versus Lg (C) is displayed in the inset of Fig. 4c. And the correlation coefficient R of detecting NO_2 sensor is 0.993 with range 1-10 ppm at low operating temperature of 110 °C. The value of β towards NO_2 is about 0.958, which is very approaches to the ideal value 1.0 derived from surface interactions between chemisorbed oxygen and target gas to the n-type semiconductor.[41]

Table 1 WO_3-based gas sensing performance for NO_2. Concentrations (*C*), operating temperature (*OT*, °C), sensitivity (*S*), response time (t_{res}, s), recovery time (t_{rec}, s), existing problems (*Prob.*), and Reference (*Ref.*).

Morphology	*C*	*OT*	*S*	t_{res}	t_{rec}	*Prob.*	*Ref.*
Self-supported	10 ppm	110	20.5	23	11		Present work
Nanorods	10 ppm	200	209	-	-	high OT, none t_{res} , t_{rec}	[6]
Square-like	1 ppm	125	150	210	90	long t_{res} , t_{rec}	[36]
Lamellae	0.5 ppm	200	150	-	-	high OT, none t_{res} , t_{rec}	[37]
Nanowire arrays	1 ppm	25	3.5	3	~150	long t_{rec}	[42]
Flower-like	40 ppb	90	80	720	~1000	long t_{res} , t_{rec}	[43]

Fig. 4c presents the typical responses of the WO_3 annealed at 300 °C to 1-10 ppm NO_2 concentrations at 110 °C. It indicates the relationship between time dependence and the responses with changing NO_2 concentrations. As the time for the sensor output to reach 90 % of its maximum response with switching on or off the different gas in a step function was defined as the response time and recovery time, respectively. As measured and depicted in Fig. S5b†, the response time and recovery time is approximately 23 s and 11 s, respectively, to 10 ppm NO_2 at optimum operating temperature of 110 °C. In order to compare the WO_3-based gas sensing properties at a certain concentrations of NO_2 in our present work and those reported in the literatures, Table 1 lists the morphology, operating temperature (*OT*), sensitivity (*S*), response time (t_{res}), recovery time (t_{rec}), existing problems (*prob.*), etc. in details. It is observed that the sensor based on hierarchical 3D WO_3 exhibits a relatively low working temperature, high response, and rapid response and recovery speed. The reasons for the high response of the sensor to NO_2 will be discussed at the section of gas sensing mechanism.

Practical applications require that gas sensors have strong sensor response, and quick response and recovery time, besides these, they need to present rather high selectivity to other harmful gases. The selectivity of the WO_3 to 10 ppm NO_2, 10 ppm acetone, and 100 ppm ether, methanol, NH_3, and ethanol are also studied at the operating temperature of 110 °C, as shown in Fig. 4d. It can be found that the WO_3 has response to 10 ppm acetone and 100 ppm ether to some degree, but slight response to 100 ppm methanol, NH_3, and ethanol gases, which might be ascribed to the low operating temperature of the gas sensor. Their response of the interfering gases increase with increasing the operating temperature to 170 °C (see the Fig. S6†), indicating that the temperature at 110 °C is not their optimum work temperature. In addition, Fig. 4e shows that the repetitive sensing performances of the WO_3 sensor nearly remained unchanged with detecting 1 ppm NO_2 at 110 °C, 2 ppm NO_2 at 110 °C, and 10 ppm acetone at 140 °C for seven cycles. It exhibits a highly reproducible response with a slight fluctuation, *i.e.* the sensors are still very stable. Therefore, the WO_3-based sensor has well selectivity and stability to NO_2 gas at 110 °C, confirming its possible application for efficient and selective detection of highly toxic NO_2 gas at low operating temperature.

3.4 Mechanisms of gas sensing properties

For the gas sensing mechanism of most *n*-type semiconductor, the change in resistance is primarily caused by the adsorption and desorption of gas molecules on the material surface.[44] When the sensor is exposed to air, as illustrated in Fig. 5a, the WO_3 will

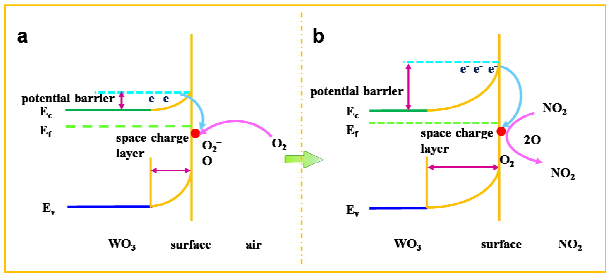

Fig. 5 Schematic diagram of the proposed response mechanism of our WO_3-based sensor to NO_2: (a) in air and (b) in the tested gas. (E_c: the bottom edge of conduction band, E_f: Fermi level, E_v: the top edge of valence band).

chemisorb oxygen molecules on their surface to transform various chemisorbed oxygen species (O_2^-, O^-) by capturing electrons from the conduction band and result in the formation of an electron-depleted space charge region on the surface, as represented in Eqs. (1)-(3).[6, 42] Owing to the different operating temperature, the primary existence of oxygen ions is different. When under 100 °C, oxygen ions exist in the form of O_2^-, or O^- when temperature between 100 and 300 °C.[6] A stable surface oxygen concentration is realized with supplying a basic electrical resistance in air. When NO_2 is introduced, as shown in Fig. 5b, the various chemisorbed oxygen ion on the surface will react with NO_2, and meanwhile, the electrons are captured by NO_2 from conductance band owing to its unique electrophilic property to produce adsorbed $NO_2^-{}_{(ads)}$, as shown in Eqs. (4) and (5). This process decreases the electron concentration on the surface, thicken the depletion layer, and raise the potential barrier, resulting in the increase of the sensor resistance. When turning off the NO_2 gas and refreshed by air, the $NO_2^-{}_{(ads)}$ ions capture electrons and desorb from the surface (see Eq. (6)), leading to the gas sensor recover to the initial condition. Thus, one cycle of the NO_2 detection is over and the sensor is ready for the next cycle.

$$O_{2\,(gas)} \rightarrow O_{2\,(ads)} \quad (1)$$

$$O_{2\,(ads)} + e^- \rightarrow O_2^-{}_{(ads)} \quad (2)$$

$$O_2^-{}_{(ads)} + e^- \rightarrow 2O^-{}_{(ads)} \quad (3)$$

$$NO_{2\,(gas)} + e^- \rightarrow NO_2^-{}_{(ads)} \quad (4)$$

$$NO_{2\,(gas)} + O_2^-{}_{(ads)} + 2e^- \rightarrow NO_2^-{}_{(ads)} + 2O^-{}_{(ads)} \quad (5)$$

$$NO_2^-{}_{(ads)} + 2O^-{}_{(ads)} + e^- \rightarrow NO_{2\,(gas)} + 2O^{2-}{}_{(ads)} \quad (6)$$

The reasons for the high response of our WO_3-based sensor to NO_2 are proposed here. One is the unique hierarchical structure of 3D WO_3 with relative high Brunauer-Emmett-Teller (BET) specific surface area of 72.32 m^2/g (Fig. S7†), assembled by numerous columns bundles (see Fig. 1c and 6a), sheets, junctions/interfaces (see Fig.1d and 6b), and ladder-shaped planes (see Fig. 6c). These provide abundant active sites and afford beneficial conditions for NO_2 chemical adsorption, when operating temperature is 110 °C. It is also found that the extremely loose structures with double-sided and self-supported nanocolumn bundles make the gas molecules easily spread into the sensing body, which offer highly favorable space for NO_2 diffusion. So when exposed to equal amount of NO_2 gas, more NO_2 will react with the adsorbed various oxygen ions (O_2^-, O^-), then causes the resistance of the sensor increase more rapidly and prominently than that of single morphology, thus our gas sensor exhibits a good property for detecting NO_2.

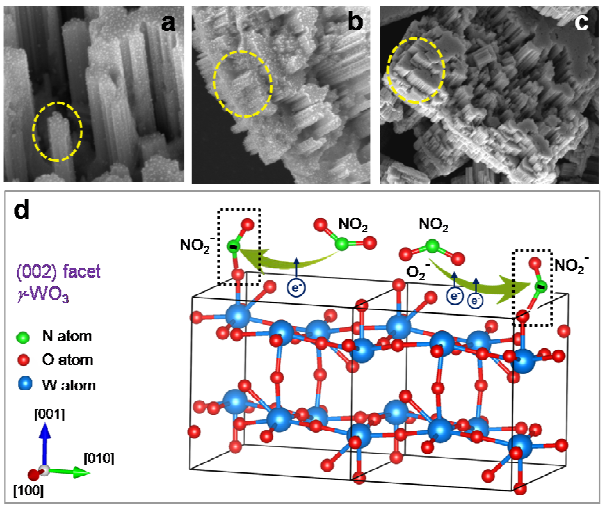

Fig. 6 (a) SEM images showing individual nanocolumn; (b) junctions /interface at the edge of double-sided WO_3; (c) the ladder-shaped plane on the top of the special structure; (d) and the illustration of NO_2 sensing mechanism on (002) facets of monoclinic WO_3 sensor.

On the other hand, our special morphology grown along [200] with largely exposed (002) facets as discussed in the TEM and XRD section may lead to high sensitivity and selectivity than that exposed other facets. We try to explain the relationship between geometrical structures of the (002) facet of γ-WO_3 and NO_2 gas molecules upon the reported,[34, 45] as illustrated in Fig. 6d. It is obvious that there are only O-terminated (002) facet contains four 1-coordinated O atoms in each WO_3 single unit cell with monoclinic structure. As performed by the Density Functional Theory (DFT) calculations, the O-terminated (001) surface is more active than a WO-terminated (001) surface.[34, 46, 47] Thus, NO_2 molecules are more easily to adsorb and react with the (002) facets, forming more oxygen vacancies and leading to a larger charge transfer between NO_2 molecules and our sensing materials, which also contribute to enhance the properties of detection NO_2 for low operating temperature, fast and selective response by using our WO_3-based sensor.

4. Conclusions

In summary, we reported an efficient one-pot hydrothermal route for preparation of 3D hierarchical structures of vertically aligned, double-sided and self-supported WO_3 column bundles at 180 ^oC for 15 h with HCl directing the morphology grown along [200], which constructed by some small nanocolumns or sheet-like shapes growing in two opposite directions from the self-supported sheet with the diameter of about hundreds of nanometers. In addition, the evolutionary process of the morphology is proposed on the basis of time-dependent experiments and different concentration of HCl. By precisely adjusting the experimental parameters, the balance between the hydrolysis rates and recrystallization rates of the WCl_6 precursors will be fabricated the special structure in our system.

The hierarchical monoclinic structure of WO_3-based sensor contains abundant active sites and loose structures beneficial conditions for gas adsorption and diffusion, which prove to be an excellent NO_2-sensing material with high sensitivity, good selectivity, rapid response (*ca.* 23 s) / recovery (*ca.* 11 s), and remarkable repeatability at a low operating temperature (~110 ^oC). A possible gas-sensing mechanism will be discussed based on largely exposed (002) facets, which the O-terminated (001) surface containing unsaturated coordinated O atoms is more active to adsorb NO_2 molecules easily and efficiently. These excellent characteristics provide numerous possible applications for our obtained materials, for example in the air pollution, particularly in easily flammable or explosive environments. Furthermore, the self-supported WO_3 materials also hold a great promise for other applications, such as noble-metal catalysts supporters, water oxidation, and electrochromic devices.

Acknowledgements

This work was financially supported by the National Basic Research Program of China (2014CB931802) and the National Natural Science Foundation of China (51272012).

References

1. Y. Li, W. Luo, N. Qin, J. Dong, J. Wei, W. Li, S. Feng, J. Chen, J. Xu, A. A. Elzatahry, M. H. Es-Saheb, Y. Deng and D. Zhao, *Angew. Chem. Int. Ed.*, 2014, **53**, 9035-9040.
2. S. Deng, V. Tjoa, H. M. Fan, H. R. Tan, D. C. Sayle, M. Olivo, S. Mhaisalkar, J. Wei and C. H. Sow, *J. Am. Chem. Soc.*, 2012, **134**, 4905-4917.
3. M. Bao, Y. Chen, F. Li, J. Ma, T. Lv, Y. Tang, L. Chen, Z. Xu and T. Wang, *Nanoscale*, 2014, **6**, 4063-4066.
4. J. Lu, A. Ma, S. Yang and K. M. Ng, *J Nanosci Nanotechnol.*, 2007, **7**, 1589-1595.
5. B. Cao, J. Chen, X. Tang and W. Zhou, *J. Mater. Chem.*, 2009, **19**, 2323-2327.
6. S. Bai, K. Zhang, R. Luo, D. Li, A. Chen and C. C. Liu, *J. Mater. Chem.*, 2012, **22**, 12643-12650.
7. S. H. Lee, R. Deshpande, P. A. Parilla, K. M. Jones, B. To, A. H. Mahan and A. C. Dillon, *Adv. Mater.*, 2006, **18**, 763-766.
8. J. Wang, E. Khoo, P. S. Lee and J. Ma, *J. Phys. Chem. C*, 2008, **112**, 14306-14312.
9. D. Ma, H. Wang, Q. Zhang and Y. Li, *J. Mater. Chem.*, 2012, **22**, 16633-16639.
10. G. Xi, J. Ye, Q. Ma, N. Su, H. Bai and C. Wang, *J. Am. Chem. Soc.*, 2012, **134**, 6508-6511.
11. J. K. Kim, J. H. Moon, T.-W. Lee and J. H. Park, *Chem. Commun.*, 2012, **48**, 11939-11941.
12. X. Chen, Y. Zhou, Q. Liu, Z. Li, J. Liu and Z. Zou, *ACS Appl. Mater. Inter.*, 2012, **4**, 3372-3377.
13. J. Yang, L. Jiao, Q. Zhao, Q. Wang, H. Gao, Q. Huan, W. Zheng, Y. Wang and H. Yuan, *J. Mater. Chem.*, 2012, **22**, 3699-3701.
14. S. K. Biswas and J.-O. Baeg, *Int. J. Hydrogen Energ.*, 2013, **38**, 3177-3188.
15. F. Amano, D. Li and B. Ohtani, *Chem. Commun.*, 2010, **46**, 2769-2771.
16. N. Wang, D. Wang, M. Li, J. Shi and C. Li, *Nanoscale*, 2014, **6**, 2061-2066.
17. Y. P. Xie, G. Liu, L. Yin and H.-M. Cheng, *J. Mater. Chem.*, 2012, **22**, 6746-6751.
18. S. Vallejos, T. Stoycheva, P. Umek, C. Navio, R. Snyders, C. Bittencourt, E. Llobet, C. Blackman, S. Moniz and X. Correig, *Chem. Commun.*, 2011, **47**, 565-567.

19. H. Nguyen Duc and S. A. El-Safty, *Nanotechnology*, 2011, **22**.
20. C. S. Rout, M. Hegde and C. N. R. Rao, *Sens. Actuators B Chem.,* 2008, **128**, 488-493.
21. L. He, Y. Liu, J. Liu, Y. Xiong, J. Zheng, Y. Liu and Z. Tang, *Angew. Chem. Int. Ed.*, 2013, **52**, 3741-3745.
22. J. Ma, J. Zhang, S. Wang, T. Wang, J. Lian, X. Duan and W. Zheng, *J. Phys. Chem. C*, 2011, **115**, 18157-18163.
23. X. L. Li, T. J. Lou, X. M. Sun and Y. D. Li, *Inorg. Chem.*, 2004, **43**, 5442-5449.
24. D. Chen and J. Ye, *Adv. Funct. Mater.*, 2008, **18**, 1922-1928.
25. J. He, H. Liu, B. Xu and X. Wang, *Small*, 2015, **11**, 1144-1149.
26. D. Chen, L. Ge, L. Yin, H. Shi, D. Yang, J. Yang, R. Zhang and G. Shao, *Sens. Actuators B Chem.*, 2014, **205**, 391-400.
27. X. Liu, L. He, J. Zheng, J. Guo, F. Bi, X. Ma, K. Zhao, Y. Liu, R. Song and Z. Tang, *Adv. Mater.*, 2015, **27**, 3273-3277.
28. M. Shibuya and M. Miyauchi, *Adv. Mater.*, 2009, **21**, 1373-1376.
29. S. Bai, K. Zhang, J. Sun, D. Zhang, R. Luo, D. Li and C. Liu, *Sens. Actuators B Chem.*, 2014, **197**, 142-148.
30. X. Zhang, X. Lu, Y. Shen, J. Han, L. Yuan, L. Gong, Z. Xu, X. Bai, M. Wei, Y. Tong, Y. Gao, J. Chen, J. Zhou and Z. L. Wang, *Chem. Commun. (Camb)*, 2011, **47**, 5804-5806.
31. X. Bai, H. Ji, P. Gao, Y. Zhang and X. Sun, *Sensors and Actuators B: Chemical*, 2014, **193**, 100-106.
32. Y. Xiong, K. Deng, Y. Jia, L. He, L. Chang, L. Zhi and Z. Tang, *Small*, 2014, **10**, 1523-1528.
33. Q. Jia, H. Ji, Y. Zhang, Y. Chen, X. Sun and Z. Jin, *J. hazard. mater.*, 2014, **276**, 262-270.
34. Q.-q. Jia, H.-m. Ji, D.-h. Wang, X. Bai, X.-h. Sun and Z.-g. Jin, *J. Mater. Chem. A*, 2014, **2**, 13602-13611.
35. X. Su, F. Xiao, Y. Li, J. Jian, Q. Sun and J. Wang, *Mater. Lett.*, 2010, **64**, 1232-1234.
36. L. You, Y. F. Sun, J. Ma, Y. Guan, J. M. Sun, Y. Du and G. Y. Lu, *Sens. Actuators B Chem.*, 2011, **157**, 401-407.
37. T. Kida, A. Nishiyama, M. Yuasa, K. Shimanoe and N. Yamazoe, *Sens. Actuators B Chem.*, 2009, **135**, 568-574.
38. S. Bai, T. Guo, D. Li, R. Luo, A. Chen and C. C. Liu, *Sens. Actuators B Chem.*, 2013, **182**, 747-754.
39. I.-D. Kim, A. Rothschild, T. Hyodo and H. L. Tuller, *Nano Lett.*, 2006, **6**, 193-198.
40. K. Mukherjee, A. P. S. Gaur and S. B. Majumder, *J. Phys. D Appl. Phys.*, 2012, **45**.
41. R. W. J. Scott, S. M. Yang, G. Chabanis, N. Coombs, D. E. Williams and G. A. Ozin, *Adv. Mater.*, 2001, **13**, 1468-1472.
42. Y. Qin, C. Liu, M. Liu and Y. Liu, *J. Alloy. Compd.*, 2014, **615**, 616-623.
43. C. Wang, R. Sun, X. Li, Y. Sun, P. Sun, F. Liu and G. Lu, *Sens. Actuators B Chem.*, 2014, **204**, 224-230.
44. H. Meixner and U. Lampe, *Sens. Actuators B Chem.*, 1996, **33**, 198-202.
45. Y. Qin, M. Liu and Z. Ye, *J. Mol. Struct.*, 2014, **1076**, 546-553.
46. L. Saadi, C. Lambert-Mauriat, V. Oison, H. Ouali and R. Hayn, *Appl. Surf. Sci.*, 2014, **293**, 76-79.
47. F. Wang, C. Di Valentin and G. Pacchioni, *J. Phys. Chem. C,* 2012, **116**, 10672-10679.

Vertically aligned, double-sided, and self-supported 3D WO_3 nanocolumn bundles for low-temperature gas sensing

The graphical and textual abstract for the contents pages

A three-dimensional (3D) hierarchical structure consisting of vertically bundled, double-sided, and self-supported WO_3 nanocolumn bundles has been successfully synthesized via acid-assisted (HCl) hydrothermal process without any templates, catalysts, or substrates. A possible formation mechanism is proposed, which involves dissolution–recrystallization and Ostwald ripening processes in concert with the structure-directing role of HCl, leading to the morphology grown along [200] with largely exposed (002) facets. The hierarchical monoclinic structure of WO_3–based sensor contains abundant active sites and loose structures beneficial conditions for gas adsorption and diffusion, which prove to be an excellent NO_2-sensing material with high sensitivity, good selectivity, rapid response (*ca.* 23 s) / recovery (*ca.* 11 s), and remarkable repeatability at a low operating temperature (~110 °C). A possible gas-sensing mechanism will be discussed based on largely exposed (002) facets, which the O-terminated (001) surface containing unsaturated coordinated O atoms is more active to adsorb NO_2 molecules easily and efficiently. The superior gas sensor properties offer a potential platform for monitoring harmful and toxic gases, especially those flammable and explosive volatile organic compounds (VOCs).